

UCRL-90475
PREPRINT

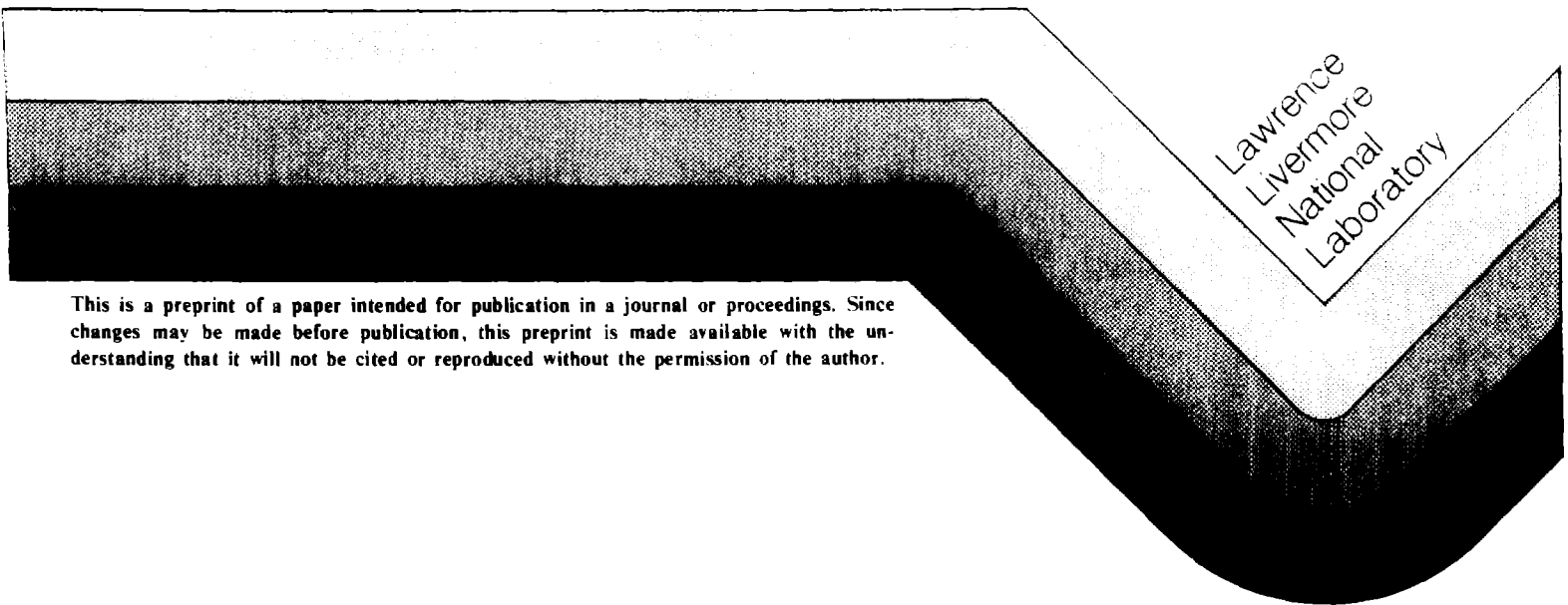
UCRL-90475
PREPRINT

DESIGN OF A HIGH-PERFORMANCE
SLIDE AND DRIVE SYSTEM FOR A
SMALL PRECISION MACHINING RESEARCH LATHE

R. R. DONALDSON
A. S. MADDUX

This paper was prepared for submittal to
CIRP Assembly
Madison, Wisconsin
August 20-25, 1984

March 1984



This is a preprint of a paper intended for publication in a journal or proceedings. Since changes may be made before publication, this preprint is made available with the understanding that it will not be cited or reproduced without the permission of the author.

DISCLAIMER

This document was prepared as an account of work sponsored by an agency of the United States Government. Neither the United States Government nor the University of California nor any of their employees, makes any warranty, express or implied, or assumes any legal liability or responsibility for the accuracy, completeness, or usefulness of any information, apparatus, product, or process disclosed, or represents that its use would not infringe privately owned rights. Reference herein to any specific commercial products, process, or service by trade name, trademark, manufacturer, or otherwise, does not necessarily constitute or imply its endorsement, recommendation, or favoring of the United States Government or the University of California. The views and opinions of authors expressed herein do not necessarily state or reflect those of the United States Government or the University of California, and shall not be used for advertising or product endorsement purposes.

DESIGN OF A HIGH-PERFORMANCE SLIDE AND DRIVE SYSTEM FOR A SMALL PRECISION MACHINING RESEARCH LATHE

R. R. Donaldson

A. S. Maddux

Lawrence Livermore National Laboratory/USA

The development of high-accuracy machine tools, principally through interest in diamond turning, plus the availability of new cutting tool materials, offers the possibility of improving workpiece accuracy for a much larger variety of materials than that addressed by diamond tools.

This paper describes the design and measured performance of a slideway and servo-drive system for a small lathe intended as a tool for research on the above subject, with emphasis on the servo-control design. The slide system provides high accuracy and stiffness over a travel of 100mm, utilizing oil hydrostatic bearings and a capstan roller drive with integral dc motor and tachometer.

Introduction

The ability to machine workpieces to ever-closer form and finish tolerances is a continuing goal in manufacturing. Over the past two decades, remarkable gains have been made for the small group of materials that are cut in a nearly ideal manner by single-crystal natural diamond tools. Taking the exceptional accuracy, finish and wear resistance of the tool as given, an accuracy improvement of perhaps two orders of magnitude has been accomplished for machine tools through a systematic cause-and-effect understanding of machine errors now known as precision engineering.

The availability of very accurate machine tools, coupled with the recent introduction of cutting tool materials having improved hardness and wear characteristics, now provides a promising basis for making significant accuracy gains in single-point cutting of a wider spectrum of workpiece materials. Support for this viewpoint comes from limited but encouraging experience in cutting non-diamond-turnable materials with the small precision lathe shown in Fig. 1 (also see Ref. 1). For example, we have been successful in cutting beryllium with a surface roughness of 25-50nm R_a and sufficient reflectivity to display optical interference fringes. The flatness achieved on a 50 mm diameter sample, 0.6 μ m, was virtually the same as that achieved on a brass witness sample, including the detailed profile shape, and hence was established as due to slide straightness error rather than the cutting process. The cutting tool used in these tests was a commercial polycrystalline cubic boron nitride material that had been sharpened to approximately a 1 μ m edge radius using a diamond-charged scribe. SEM study of the tool edge showed no detectable flank wear, although only a 2000mm² area was cut.

Our limited experience with non-diamond-turnable materials on the above lathe also indicates that the stiffness of the machine structure is an important factor. The diamond cutting process is relatively tolerant of low structural stiffness, a fact that can be used to advantage in diamond turning machine design. The lathe of Fig. 1, which is quite stiff for a small machine, has been successful in cutting tests where negative results were obtained with less stiff diamond turning machines.

In order to pursue these preliminary findings, we are designing and constructing a successor to the above machine to use for precision metal-cutting research. The general goal is to provide a numerically controlled lathe having sufficiently ideal performance as to allow study of the tool-work interaction without significant influence on accuracy from the machine. The primary limitation of the machine in Fig. 1 is the commercial slides and drives (which were originally designed for high-speed step-and-repeat applications). The present paper presents an improved slide and slide drive system, designed for this application.

The research lathe project has also been influenced by another predecessor, the Large Optics Diamond Turning Machine Project (LODTM; also see Ref. 2). Examples are the use of oil hydrostatic bearings and capstan-roller slide drives in the present work. Also, high-resolution fringe interpolation electronics developed for the LODTM laser interferometers will allow an equal control system least count of 2.5nm to be used for the research lathe.

Slide Drive Servo-Control

For high performance the design of the slide drive must be considered as a simultaneous mechanical and electronic servo-control problem. Of particular concern are the effects of cyclic disturbances that occur within the control loop hardware. The primary sources of disturbance are cyclic displacements from bearings in the drive system, voltage ripple in the dc tachometer velocity signal and torque ripple in the dc servomotor output. The design goal for the servo-control system is to reduce the resulting output disturbance to one least count of 2.5nm at slide speeds up to 0.5mm/sec (30mm/min).

As an example, consider a typical leadscrew drive system with a laser interferometer for position feedback. From a mechanical viewpoint, it may seem attractive to use a very fine-pitch screw, say $L = 1\text{mm/rev}$, directly driven by a small high-speed servomotor/tachometer unit. The primary displacement disturbance will come from the leadscrew thrust bearing; a measured value of axial motion in an assembly with precision angular contact bearings is $0.2\mu\text{m}$ (200nm) amplitude and 10 cycles per leadscrew revolution. Thus at a slide velocity of 0.5mm/sec, the disturbance will be 200 nm at a frequency of 5 Hz. A typical machine tool slide controller for leadscrew drives has a bandwidth below 5 Hz, and hence this disturbance will not be rejected by the control loop.

Several alternatives can be used to reduce the above disturbance; a reduction of $200/2.5 = 80:1$ is required to meet the design goal:

1. Reduce the disturbance amplitude.
2. Reduce the disturbance frequency via a reduced design goal slide velocity.
3. Increase the control loop bandwidth.
4. Reduce the disturbance frequency by increasing the lead/revolution.

The first alternative would require an unreasonable degree of perfection in the physical components, and the second alternative directly reduces the productivity of the machine tool.

The third alternative can contribute a fraction of the required improvement. Normal design practice requires that the control loop bandwidth be a factor of 5-10 below the first resonant frequency of the slide drive assembly, and it is difficult to increase the latter beyond a few hundred Hertz in the sizes being considered without use of exotic materials or fabrication techniques. A goal of 50 Hz control loop bandwidth was chosen for the present design.

The fourth alternative is readily achieved by use of a capstan drive, which with a roller radius R of 10-30 mm has a $2\pi R$ lead/revolution that

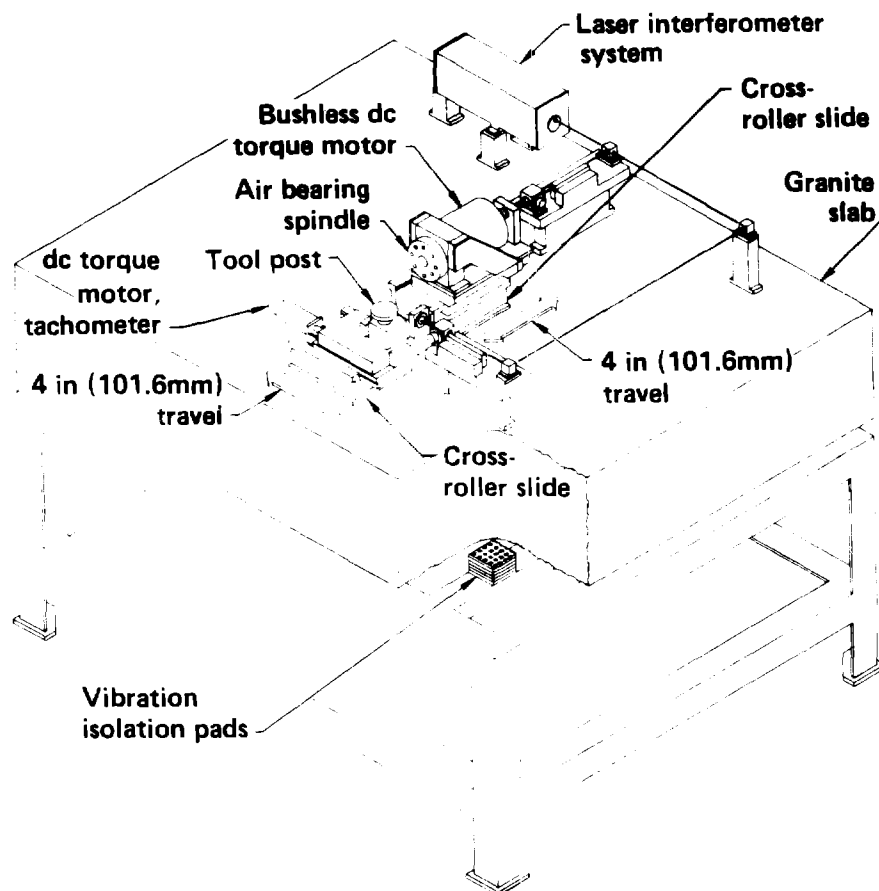


Fig. 1. Isometric view of existing small precision lathe.

is about a hundredfold larger than the above example. Since this increase in lead/revolution also reduces the frequency of the motor and tachometer ripple correspondingly, it is a primary reason for choosing a capstan drive for the present design.

Figure 2 provides a quantitative design tool for estimating the effects of the various disturbances. The derivation of Figure 2 is given in the Appendix. Each graph is a log-log (Bode) plot showing db amplitude attenuation between input and output, based on the input frequency. The top block, for example, shows the system response to the displacement input command $I(s)$, which is a two pole loop varying from 0 db at dc to -3 db at the closed-loop bandwidth f_{c1} .

To use Figure 2, the designer must first choose a value for f_{c1} , based on a combination of experience, calculation of structural resonant frequencies and measurements (if the hardware exists). The value of f_x , the unity-gain crossover frequency, is chosen as $0.75 f_{c1}$ (= 37.5 Hz for the present design).

The second Bode plot of Figure 2 shows the attenuation of tachometer ripple. The equations give the amplitude and frequency of the ripple disturbances in terms of manufacturer's data (percent ripple r_t and ripple cycles per revolution N_t) and the parameters of the application. For the present case, the values for the selected commercial tachometer are:

$$r_t = \left(\frac{0.4\% \text{ 0-pk}}{100\%} \right) \times 2 = 0.008 \text{ pk-pk}$$

$$V_s = 0.5 \text{ mm/sec} = 5 \times 10^5 \text{ nm/sec}$$

$$\omega_x = 2\pi f_x = 236 \text{ rad/sec}$$

$$N_t = 68 \text{ cycles/rev}$$

$$R = 12.7 \text{ mm}$$

$$\text{Then } (A_t)_{in} = \frac{0.008 \times 5 \times 10^5}{236} = 17 \text{ nm}$$

$$f_t = \frac{68 \times 0.5}{2\pi \times 12.7} \approx 0.197 \text{ Hz} = \frac{f_x}{88}$$

Entering the second Bode plot at $f_x/88$ gives a divisor of 8.8, so the output amplitude is

$$(A_t)_{out} = \frac{17}{8.8} = 1.9 \text{ nm}$$

For the motor, the values needed for the equations are

$$r_t = \left(\frac{7\% \text{ 0-pk}}{100\%} \right) \times 2 = 0.14 \text{ pk-pk}$$

$$N_m = 31 \text{ cycles/revolution}$$

$$J = J_{\text{rot}} + mR^2 = 5.15 \text{ N-mm-sec}^2$$

$$F_s = 5 \text{ N}$$

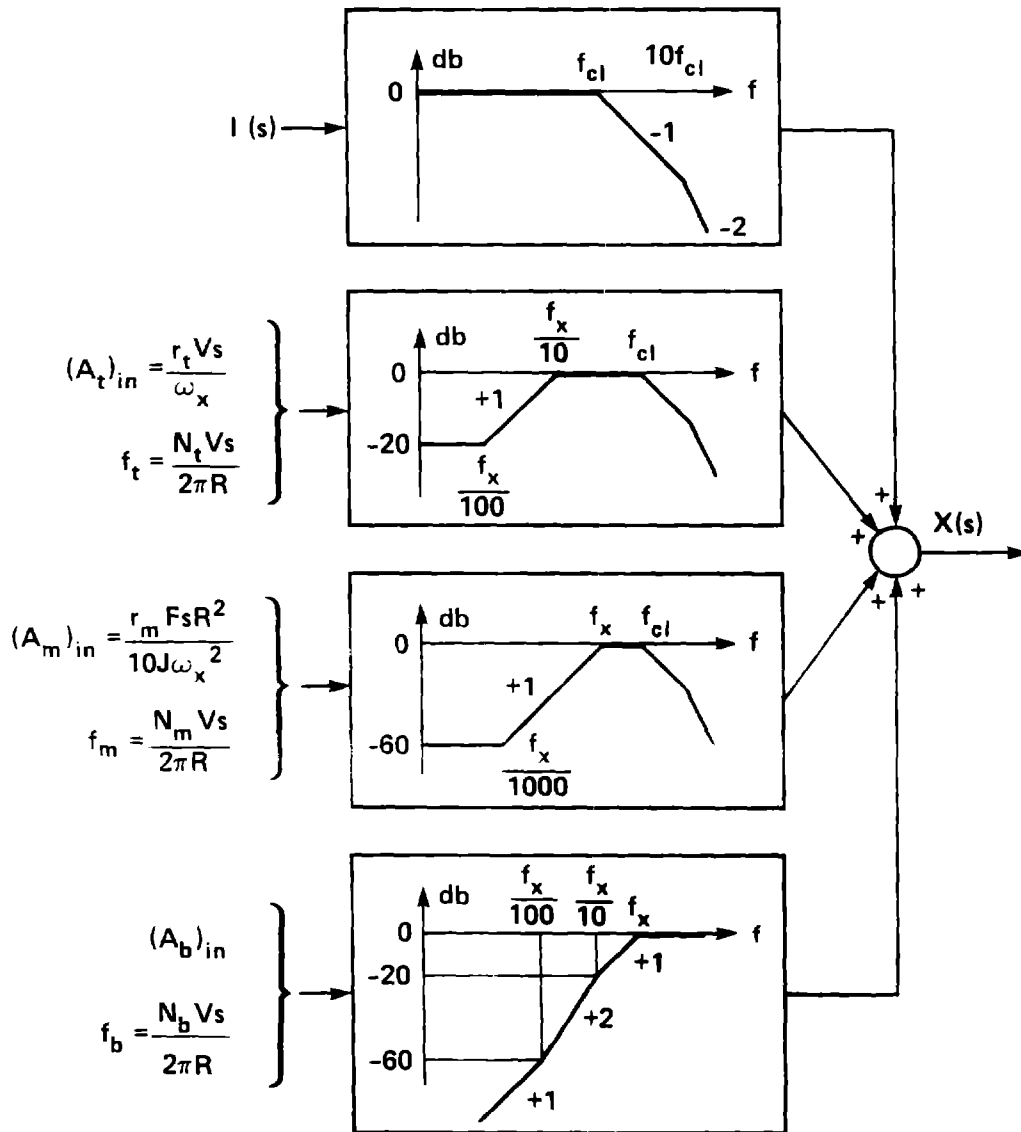


Fig. 2. Servo-loop disturbance rejection diagram.

Since the accuracy goal is required only during a fine finish cut, a small value has been chosen for F_S .

$$\text{Then } (A_m)_{in} = \frac{0.14 \times 5 \times (12.7)^2}{10 \times 5.15 \times (236)^2} = 38.7 \text{ nm}$$

$$f_m = \frac{31 \times 0.5}{2\pi \times 12.7} = 0.194 \text{ Hz} = \frac{f_x}{193}$$

Examining the third Bode plot at $f_x/193$ gives a divisor of 193, so

$$(A_m)_{out} = \frac{38.7}{193} = 0.2 \text{ nm}$$

It is evident that the rejection characteristic for motor torque ripple is much more favorable than for tachometer ripple.

For bearing ripple, the amplitude $(A_b)_{in} = 0.2 \mu\text{m} = 200 \text{ nm}$ will be used from the earlier example, together with the rotational frequency, $N_b = 10$ cycles/revolution. Hence

$$f_b = \frac{10 \times 0.5}{2\pi \times 12.7} = 0.63 \text{ Hz} = \frac{f_x}{598}$$

From the bottom Bode plot, the attenuation is -60 db (10^{-3}) at $f_x/100$, so

$$(A_b)_{out} = 200 \times \frac{10^{-3}}{5.98} = 0.03 \text{ nm}$$

The rejection characteristic for bearing ripple is also quite favorable when the input frequency is low relative to f_c .

The sum of the calculated output disturbance amplitudes is seen to be 2.13nm (if all were to coincide in phase), within the design goal of 2.5nm.

A few further comments are necessary regarding the choice of the roller radius R in a capstan drive. Except for increasing the input amplitude of the motor torque ripple, the above analysis favors larger values of R . The fact that the capstan roller is a mechanical element subjected to bending and torsion at the drive bar interface also indicates a larger R to increase the structural resonant frequency (and to reduce the interface contact stress for a given normal load). However, for a given maximum thrust force to be exerted by the slide, the required motor torque increases in proportion to R , and could lead to a motor of unreasonable size. Also, as R increases, the tachometer rotational speed decreases, leading to signal/noise difficulties at very low slide velocities (as will be required when a contouring cut is nearly tangent to either machine axis). Comparing this design with that of the LODTM capstan drives, the latter used twice as large a roller radius but also used a larger tachometer with five times the voltage sensitivity, indicating a 2.5:1 higher minimum slide velocity for the present system. This should be adequate since LODTM is a much larger, slower-moving machine (also see Ref. 3).

Slide Drive Mechanical Design

Having selected a capstan drive as well as specific dc tachometer and motor components on the basis of servo-control considerations (and general size limitations), the capstan drive design is largely a packaging problem; see Fig. 3.

The tachometer and motor are both of frameless design with 92mm outside diameter. They are contained in a non-magnetic housing of 140mm height, with the rotating components clamped to the capstan roller shaft. A mu-metal shield encloses the tachometer for rf noise suppression.

The maximum thrust force to be exerted by the slide drive was chosen as 100N; adequate torque capacity was considered in the motor selection. Also, using a conservative friction coefficient of 0.1 at the roller interface, a preload force of 1000N was chosen. The roller is supported by a pair of precision angular contact bearings and the preload force is applied to the drive bar by an air-bearing pad mounted on a pivot ball for self-alignment. The cylindrical roller and flat drive bar form a line contact. A slight crowning is desirable to avoid stress-risers at the ends of the line contact, but no difficulty has been experienced without crowning, using 440C material of 58-60 R_c hardness. An estimate of the contact stress can be obtained from Ref. 4. Ref. 5 contains a more elaborate analysis for elliptical contact zones (i.e., with crowning), and includes an expression for tangential shear stiffness of the contact zone.

The drive bar connects to the slide through flexures designed to maintain high axial stiffness while allowing a few milliradians of angular misalignment. There are two flexures at right angles; each consists of opposing edge-to-center wire EDM slots that leave a central web about 0.25mm in width and axial length across the full bar depth.

Slideway Mechanical Design

Hydrostatic (externally pressurized oil-film) bearings are used for the linear slideway bearings, again based on experience from LODTM. Compared to gas-film bearings, hydrostatic bearings have the advantages of better damage resistance, higher viscous damping in the drive direction as an aid in the servo-control compensation, and a much higher lateral (squeeze-film) damping that improves the dynamic characteristics of the machine structure. These factors are sufficient to outweigh the difficulties in fluid pressurization and collection.

The bearing configuration requires careful consideration. For high stiffness a small slide requires a captured (preloaded) design. It is attractive to use prismatic structural elements with flat bearing surfaces, but approaches employing a C-frame structure tend to deflect more from the preload force than the desired operating clearance, making fabrication difficult. DeGast (Ref. 6) has minimized this effect, but at the expense of a relatively small bearing area, requiring active flow restrictors for high stiffness.

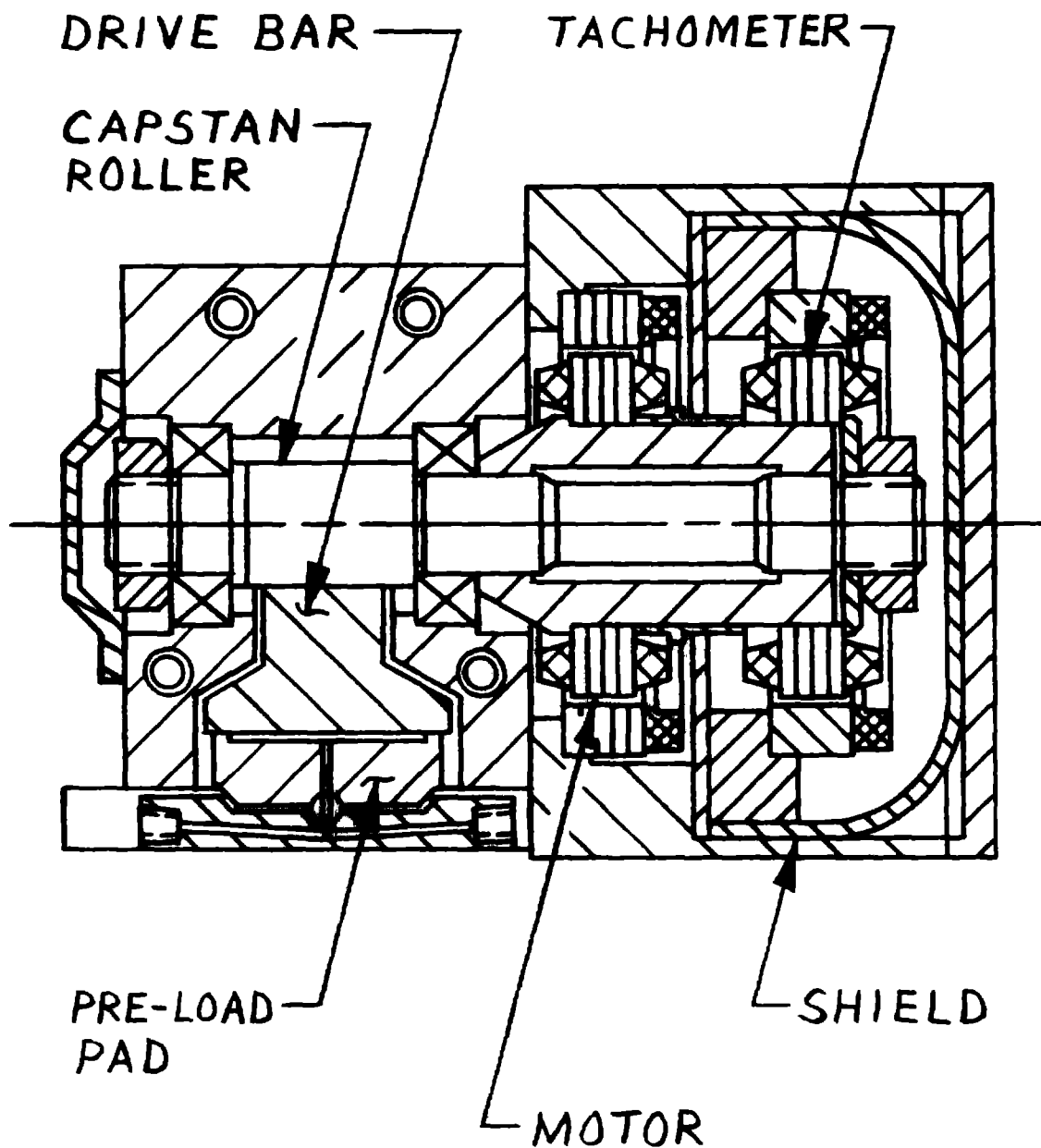


Fig. 3. Cross-section of capstan drive assembly.

The approach taken in the present design is to use a pair of cylindrical support rods as shown in Fig. 4. The bearings are full 360° journal bearings having no unidirectional preload deflection. The primary disadvantage of this design is the obvious over-constraint of the bearings. This has been reduced by attaching the cylindrical rods to their base with axial end-clamps rather than with locating bores. During assembly, the bearings are pressurized to center the rods in the carriage bearings prior to tightening the axial clamps. With this arrangement, the only significant alignment error is

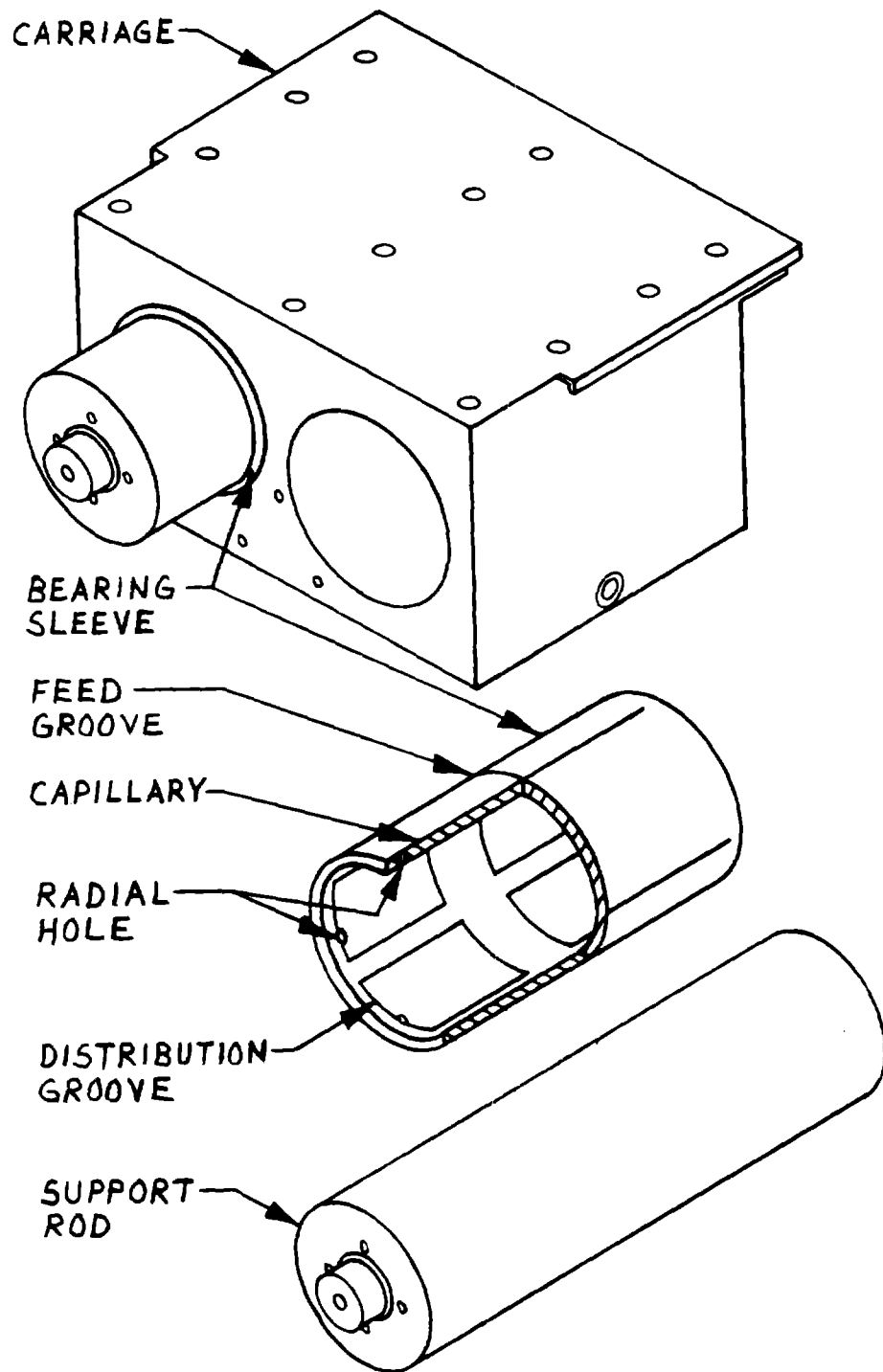


Fig. 4. Partially disassembled isometric view of carriage, hydrostatic bearings and support rods.

nonparallelism of the two bearing bores in the plan view. (Nonparallelism in the side view causes carriage roll, but only second-order changes in clearance.) If the carriage is at mid-travel during assembly it is easily shown that mechanical interference will not occur at the extremes of travel unless the angle between the bearing bores reaches twice the diametral clearance divided by the total slide travel. For the present design, with $12.5\mu\text{m}$ diametral clearance and 100mm total travel, the angle limit is $250\mu\text{rad}$. With a bore length of 150mm, this amounts to a difference in center distances of $37.5\mu\text{m}$ at opposite ends of the carriage. For precision jig-grinding, a tolerance of 5% of this value ($\sim 2\mu\text{m}$) is not unreasonable.

For high structural stiffness, the support rod diameter is as large as feasible in terms of the overall slide dimensions, giving rods of 75mm diameter by 250mm long. As a space-saving measure, the capillary restrictors are shallow longitudinal grooves on the outside of the bearing sleeve, which is an interference fit in the carriage, as shown in Fig. 4. Otherwise the bearings have a typical four-pad design. The pad center area is not recessed, to increase the shear drag and squeeze-film area. The slide base is a five-sided box frame designed to resist lateral loads; it is attached to the granite machine base.

As with LODTM, to avoid pump vibration, compressed air at 0.83 MPa pressurizes the bearing oil supply tank, with two tanks and a solenoid switching scheme for periodic refilling.

Measured Slideway Performance

Fig. 5a shows the straightness of travel of an assembled slideway, measured in the horizontal direction at the spindle centerline height of 85mm above the carriage top. Over 100mm of travel, the deviation is 200nm in the form of a smooth arc. The machine control computer will have the ability to store and correct for repeatable straightness errors.

Fig. 5b shows the dynamic response of the slide to a step change in force. The force and displacement were both in the vertical direction at the center of the carriage, which was at mid-travel. For a force change (weight removal) of 118N, there is an immediate elastic response from the structure of 145nm, giving a stiffness value of 0.81N/nm ($0.81 \times 10^6\text{N/mm}$). This is followed by an exponential-decay response of approximately equal magnitude from the interaction of the hydrostatic bearing stiffness and the squeeze-film damping, having a time constant of about 12 seconds.

Returning to Fig. 5a, it can be seen that at the start and end of the straightness movement, performed at 25mm/min, there is evidence of about 20nm of transient behavior. This behavior is probably a hydrodynamic steering due to imperfections in the bearing geometry (slopes in the direction of travel), followed by a recovery transient as in Fig. 5b. Therefore the system would benefit from reducing both the hydrodynamic and squeeze-film effects by about one order of magnitude. This could be accomplished with a lower oil viscosity, but at the expense of also reducing the beneficial viscous drag in

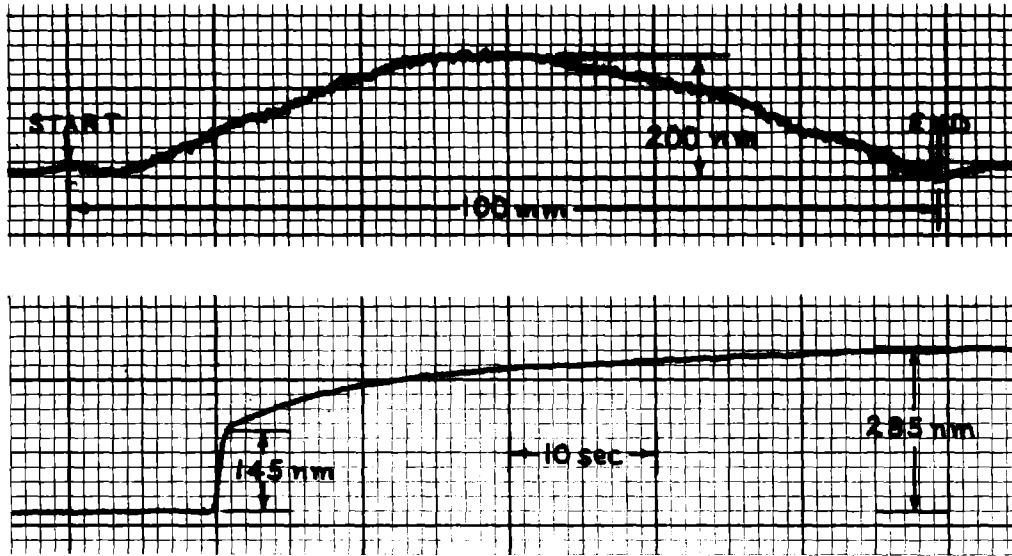


Fig. 5. a) Measured slide straightness error in full travel;
 b) Step response of carriage to 118N vertical force.

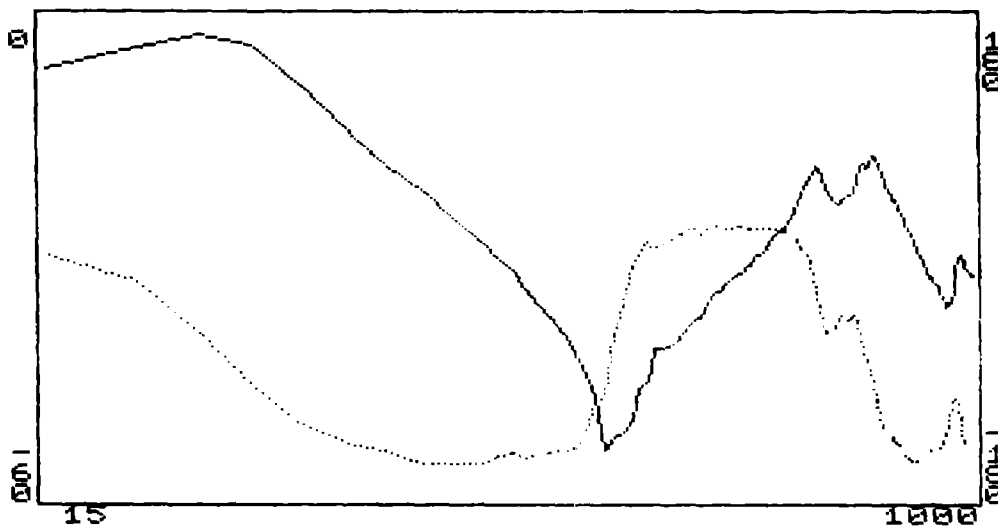


Fig. 6. Motor-tachometer transfer function without compensation. Abscissa, frequency f in Hertz (log scale); left ordinate, gain G in db (heavy curve); right ordinate, phase ϕ in degrees (light line). Numerical values near corners are full ranges of f , G and ϕ .

the drive direction. A more desirable (but difficult) option would be to cross-hatch the large pad center areas with narrow grooves, which would prevent motion-induced pressures while not decreasing the viscous drag materially. The oil viscosity during these tests was about 100 cs, yielding a flow rate of 0.4 l/h.

Servo-Loop Compensation

Figs. 6-8 show computer plots of the servo compensation results. In each, frequency is shown logarithmically on the horizontal axis, with the range of frequencies shown in Hertz. The solid gain curve is read on the left vertical axis in decibels (db), while the dashed phase curve is read on the right vertical axis in degrees. When cursor lines are present, additional values are shown for their intersection.

Fig. 6 shows the transfer function measurement between the voltage input to the motor servo amplifier (essentially the motor torque T) and the tachometer output ω with no compensation. The gain curve shows a large drop (-53db) at 196Hz, followed by peaks nearly 40db higher at 500-600Hz. Also, the phase shift is about 150° in the 100-150Hz region. This behavior is due to two inertias, the motor/tach and the carriage, that are connected by a spring. The spring includes drive bar and flexure extension, shear in the friction interface zone and deflection of the capstan roller shaft and bearings.

The velocity loop compensator consists of three cascaded blocks. The first block has real poles with one integrator with 73.7db gain at 0.01Hz, plus four zeroes to reduce the phase shift below 200Hz. The other blocks are unity-gain bridged-tee filters with frequencies of 532 and 2130Hz, both with damping at 25% of critical. The pole and zero frequencies (in Hz) are given in Table 1.

Table 1. Velocity Loop Compensator Design

	Zeroes		Poles	
	Real	Imag	Real	Imag
Block #1	-50	0	-1E-06	0
	-50	0	-220	0
	-50	0	-220	0
	-50	0	-220	0
			-10000	0
Block #2	-138	532	-129	0
	-138	-532	-2346	0
Block #3	-550	2130	-516	0
	-550	-2130	-9384	0

Fig. 7 shows the same measured T vs. ω open loop transfer function with the above compensator installed. The gain is set at unity (0db) at 143Hz, where the phase margin is 57° .

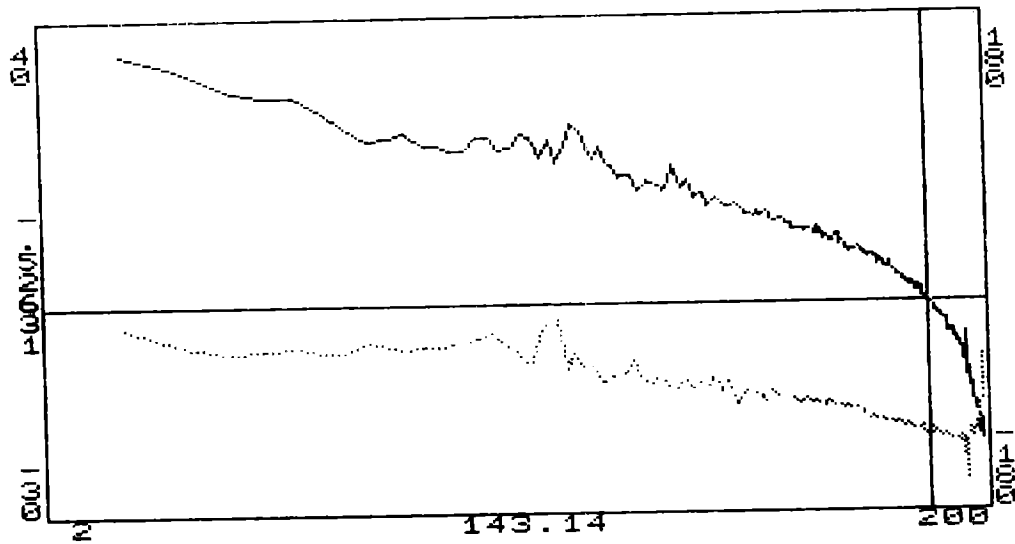


Fig. 7. Motor-tachometer transfer function with velocity compensation, open loop. Numerical values at center of ordinate and abscissa are coordinates at cursor line intersection.

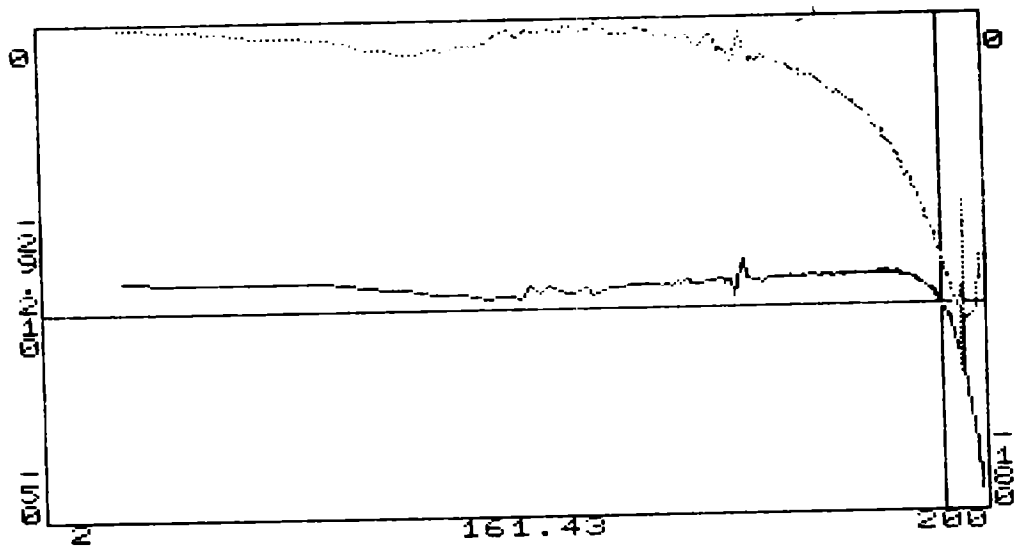


Fig. 8. Closed velocity loop motor-tachometer transfer function.

Fig. 8 also shows T vs. ω , but with the velocity control loop closed. The gain curve is flat within 3db up to 161Hz, while the phase shift is less than 15° up to 70Hz, reaching 90° at 161 Hz.

The factor of ultimate concern, of course, is the velocity and position response of the carriage. At this writing, the laser interferometer hardware for carriage position measurement was not installed, making carriage response data unavailable. However, the results of Fig. 8 coupled with analogous experience from the LODTM capstan drive system indicates that a closed loop position bandwidth at or near 50Hz remains a reasonable goal.

Conclusions

By combining mechanical and servo-control design techniques, it is possible to produce a small slideway and drive system combining excellent performance in terms of static and dynamic stiffness, straightness of travel and control system bandwidth. The resulting hardware should provide an advance in precision machining, especially with regard to research into producing closer-tolerance parts with new tool and workpiece material combinations.

Acknowledgements

The method described in the Appendix is adapted from informal notes by Dr. Howard K. McCue, LODTM Electronics Project Engineer. Much of the meticulous work of fabricating and assembling the mechanical hardware was performed by Mr. Pete Davis. Funding for this work was provided by the Engineering Research Program of the Lawrence Livermore National Laboratory.

References

1. Thompson, D.C., Chrislock, J.L. and Newton, L.E., "Development of an Inexpensive, High-Accuracy Diamond Turning Machine," Precision Engineering, Vol. 4, No. 2, April 1982, pp. 73-77.
2. Donaldson, R.R. and Patterson, S.R., "Design and Construction of a Large, Vertical Axis Diamond Turning Machine," Proceedings SPIE, Vol. 433, August 1983, pp. 62-67.
3. McCue, H.K., "The Motion Control System for the Large Optics Diamond Turning Machine (LODTM)," Proceedings SPIE, Vol. 433, August 1983, pp. 68-75.
4. Timoshenko, S., Strength of Materials, Part II, 3rd. ed., D. Van Nostrand Co., New York, NY, 1956, pp. 342-343.
5. Donaldson, R.R., et al, Large Optics Diamond Turning Machine Technical Report, LLNL publication UCAR-10075-1, April 1981, pp. 2-9.
6. DeGast, J.G.C., "A New Type of Controlled Restrictor (M.D.R.) for Double Film Hydrostatic Bearings and Its Application to High-Precision Machine Tools," 7th Int'l M.T.D.R. Conf., September 1966.

APPENDIX

This appendix presents a simplified but useful approach for calculating slide position errors due to torque, velocity and position disturbances. Fig. A-1 shows a linear model consisting of dc torque motor and amplifier (gain K) driving a simple inertia J , with an inner velocity loop (tachometer gain K_t) and an outer position loop (gain K_p). $I(s)$ and $X(s)$ are respectively the displacement input command and output response; $G_{cp}(s)$ and $G_{ct}(s)$ are the position and tachometer compensators. The torque, velocity and position disturbances are respectively $T_d(s)$, $W_d(s)$ and $X_d(s)$.

The validity of the model of Fig. A-1 depends, first, on keeping f_{c1} an order of magnitude below the structural resonant frequencies. Experience with LODTM capstan drives has shown that the principal non-linearities appear in the tachometer loop, due to brush friction and a torsional magnetic spring effect. If the tachometer, motor and drive roller form a tightly coupled mechanical package with high natural frequency, the non-linearities can be "linearized" by high tachometer loop gain and are not significant in the position loop performance. This approach, and hence this model, would probably be less successful for leadscrew drives.

To calculate the position errors, the position and tachometer compensators must be known. Fig. A-2b shows a conservative design for $G_{cp}(s)$, where f_x is the crossover frequency (open loop gain equal to unity), set at 75% of f_{c1} . The high frequency gain K_{cp} is set by requiring

$$\left| \frac{K_{cp} K_p R}{K_t s} \right| = 1 \quad (A-1)$$

when $|s| = \omega_x = 2\pi f_x$, or

$$K_{cp} = \frac{\omega_x K_t}{R K_p} \quad (A-2)$$

Fig. A-3 shows similar information for the tachometer compensator $G_{ct}(s)$. The closed-loop bandwidth is conservatively assumed to be ten times f_{c1} (smaller ratios are usually possible). Also, additional low-frequency gain is added to minimize the nonlinearities mentioned above. Otherwise, the compensators are similar; K_{ct} is set by requiring

$$\left| \frac{K_{ct} K_t}{Js} \right| = 1 \quad (A-3)$$

when $|s| = 10 \omega_x$, or

$$K_{ct} = \frac{10 \omega_x J}{K K_t} \quad (A-4)$$

$$\text{where } J = J_{rot} + mR^2 \quad (A-5)$$

is the inertia at the drive motor and R is the roller radius.

The first three Bode plots of Figure 2 can be obtained by rearranging the block diagram of Fig. A-1 into that of Fig. A-4. The top Bode plot is simply the assumed closed-loop response. For the second Bode plot, note that in the 0 db region, the tachometer disturbance input $W_d(s)$ is multiplied by $K_t/K_{cp}K_p$ (from Fig. A-4 and A-3) and from Eq. (A-2),

$$\frac{K_t}{K_{cp} K_p} = \frac{R}{\omega_x} \quad (A-6)$$

Similarly, the torque disturbance input is multiplied by (using Eqs. A-4 and (A-3)),

$$\frac{1}{K K_{cp} K_{ct} K_p} = \frac{R}{10 J \omega_x^2} \quad (A-7)$$

If the amplitudes of the tachometer and motor disturbances are based on percentage ripple values, then

$$W_d = \left(\frac{\% \text{ ripple}}{100\%} \right)_t \times \omega_t = \frac{r_t V_s}{R} \quad (A-8)$$

$$T_d = \left(\frac{\% \text{ ripple}}{100\%} \right)_m \times T_m = r_m F_s R \quad (A-9)$$

The products of the input amplitudes and their multipliers yields the results shown in Figure 2,

$$W_d \frac{K_t}{K_{cp} K_p} = \frac{r_t V_s}{\omega_x} \quad (A-10)$$

$$T_d \frac{1}{K K_{cp} K_{ct} K_p} = \frac{r_m F_s R^2}{10 J \omega_x^2} \quad (A-11)$$

Finally, the input frequencies are simply the ripple frequencies N_t and N_m in cycles per revolution times the angular speed in Hz,

$$f_t = \frac{N_t V_s}{2 \pi R} \quad (\text{A-12})$$

$$f_m = \frac{N_m V_s}{2 \pi R} \quad (\text{A-13})$$

Finally, the attenuation of the position disturbance input $X_d(s)$ must be considered. Fig. A-5a shows the block diagram, which has a closed loop transfer function

$$\frac{X(s)}{X_d(s)} = \frac{1}{1 + K_p G(s)} \quad (\text{A-14})$$

where $G(s)$ is defined by comparison with Fig. A-1. Fig. A-5b shows the closed-loop position gain $(1 + K_p G(s))$ term; the inverse of the latter term is the fourth Bode plot of Fig. 2. The input amplitude A_b must be based on an estimate or measurement of the bearing error motion, while N_b is the cycles per revolution of this motion.

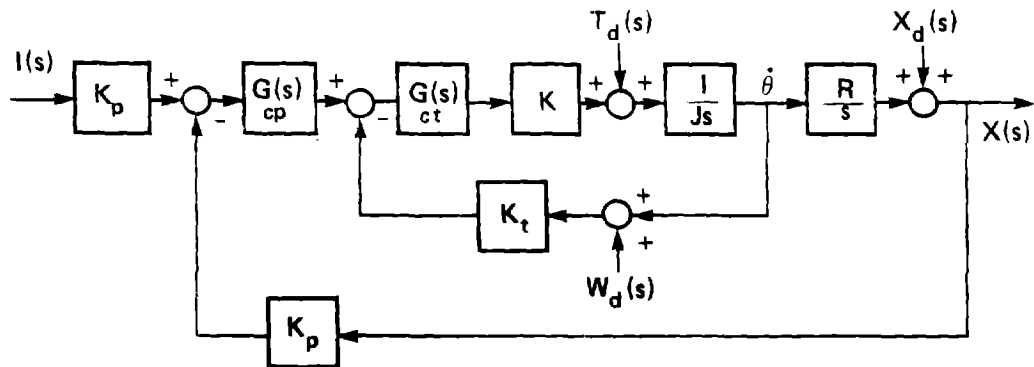


Fig. A-1. Slide servo-control block diagram including disturbance inputs.

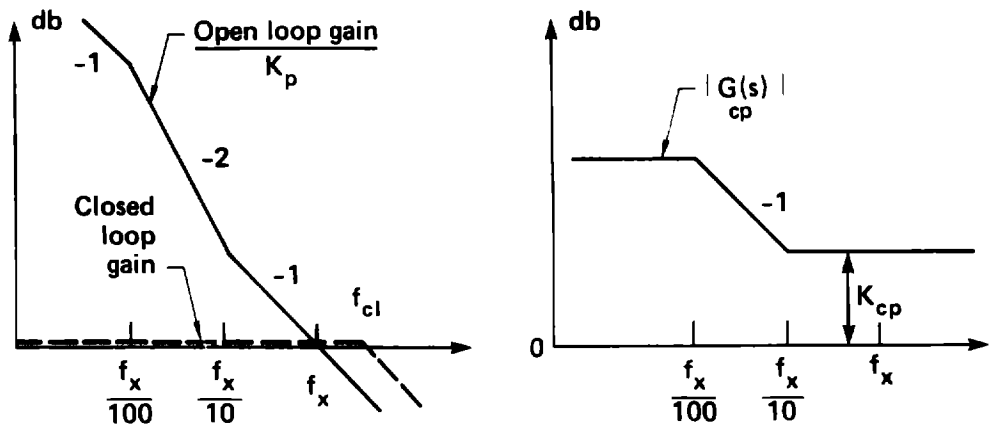


Fig. A-2. a) Position open and closed loop gain plots;
 b) Position loop compensator.

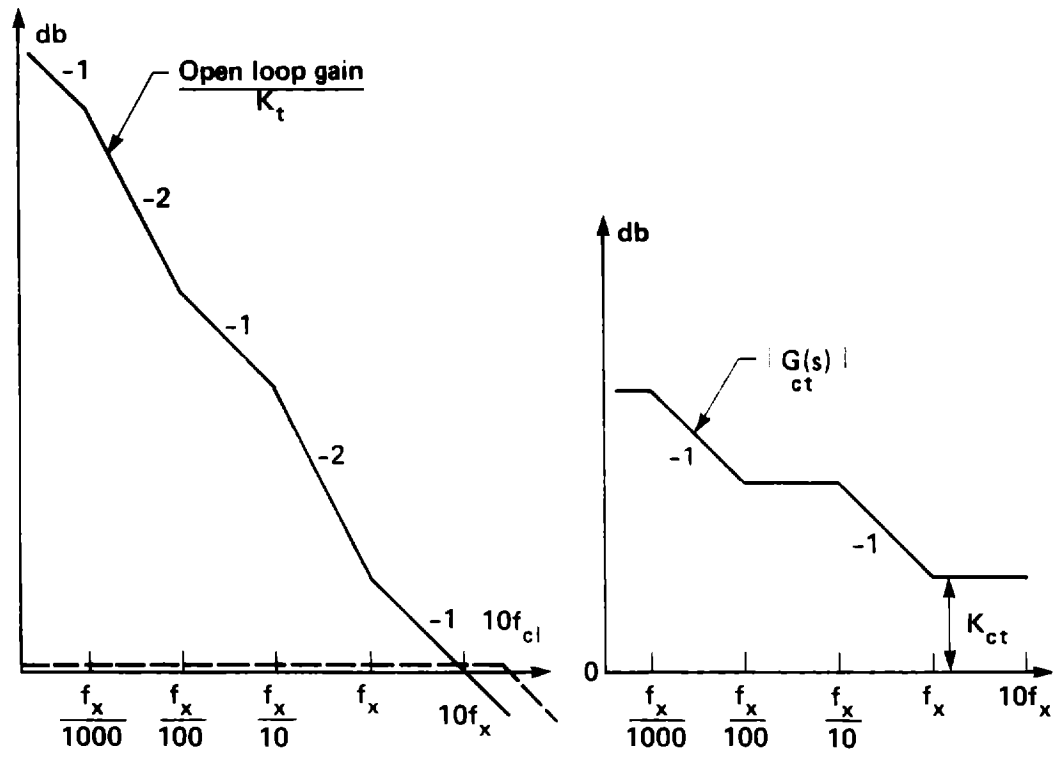


Fig. A-3. a) Velocity open and closed loop gain plots;
 b) Velocity loop compensator.

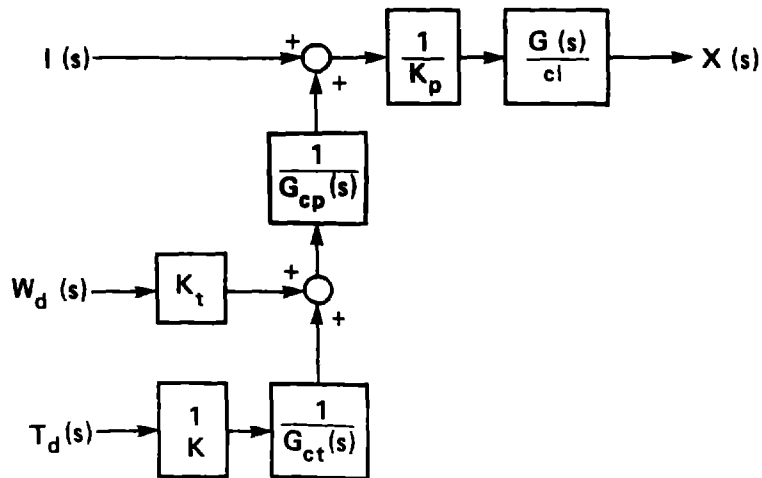


Fig. A-4. Rearranged block diagram for velocity and torque disturbances.

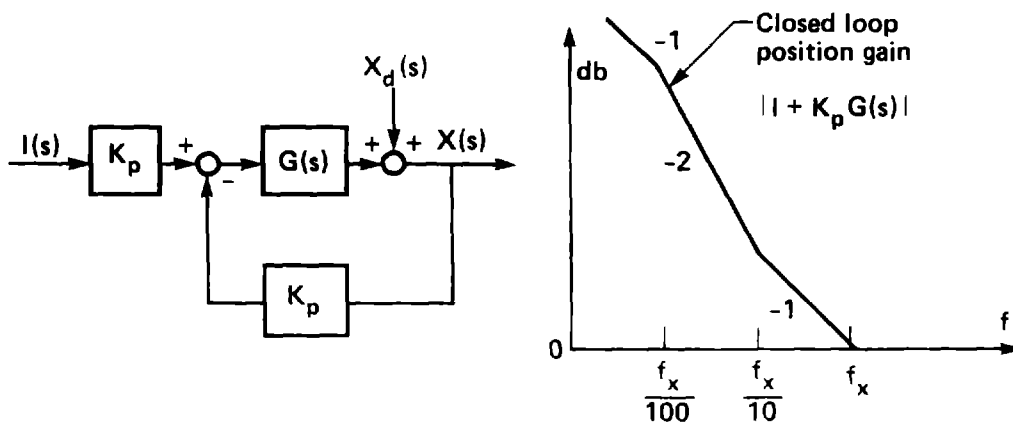


Fig. A-5. a) Position disturbance block diagram;
b) Closed loop position gain plot.

Work performed under the auspices of the U.S. Department of Energy by the Lawrence Livermore National Laboratory under contract number W-7405-ENG-48.

DISCLAIMER

This document was prepared as an account of work sponsored by an agency of the United States Government. Neither the United States Government nor the University of California nor any of their employees, makes any warranty, express or implied, or assumes any legal liability or responsibility for the accuracy, completeness, or usefulness of any information, apparatus, product, or process disclosed, or represents that its use would not infringe privately owned rights. Reference herein to any specific commercial product, process, or service by trade name, trademark, manufacturer, or otherwise, does not necessarily constitute or imply its endorsement, recommendation, or favoring by the United States Government or the University of California. The views and opinions of authors expressed herein do not necessarily state or reflect those of the United States Government or the University of California, and shall not be used for advertising or product endorsement purposes.